Acta Mechanica Sinica (2014) 30(5):628–635
DOI 10.1007/s10409-014-0033-x

RESEARCH PAPER

Time-optimal rendezvous transfer trajectory for restricted cone-angle range solar sails

Jing He · Sheng-Ping Gong · Fang-Hua Jiang · Jun-Feng Li

Received: 28 October 2013 / Revised: 16 December 2013 / Accepted: 24 February 2014

Abstract The advantage of solar sails in deep space exploration is that no fuel consumption is required. The heliocentric distance is one factor influencing the solar radiation pressure force exerted on solar sails. In addition, the solar radiation pressure force is also related to the solar sail orientation with respect to the sunlight direction. For an ideal flat solar sail, the cone angle between the sail normal and the sunlight direction determines the magnitude and direction of solar radiation pressure force. In general, the cone angle can change from 0° to 90°. However, in practical applications, a large cone angle may reduce the efficiency of solar radiation pressure force and there is a strict requirement on the attitude control. Usually, the cone angle range is restricted less more than an acute angle (for example, not more than 40°) in engineering practice. In this paper, the time-optimal transfer trajectory is designed over a restricted range of the cone angle, and an indirect method is used to solve the two point boundary value problem associated to the optimal control problem. Relevant numerical examples are provided to compare with the case of an unrestricted case, and the effects of different maximum restricted cone angles are discussed. The results indicate that (1) for the condition of a restricted cone-angle range the transfer time is longer than that for the unrestricted case and (2) the optimal transfer time increases as the maximum restricted cone angle decreases.

Keywords Solar sail · Time-optimal rendezvous · Indirect method · Restricted cone-angle range

The project was supported by the National Natural Science Foundation of China (11272004 and 11302112) and China's Civil Space Funding.

J. He · S.-P. Gong (✉)$_1$ · F.-H. Jiang · J.-F. Li (✉)$_2$
School of Aerospace, Tsinghua University,
100084 Beijing, China
e-mail$_1$: gongsp@tsinghua.edu.cn
e-mail$_2$: lijunf@tsinghua.edu.cn

1 Introduction

Solar sails consist of large-area reflective films that harvest thrust by reflecting solar photons without fuel consumption. Since the early 1990s, solar sails have aroused increasing interest in both theoretical and experimental communities. The launch of IKAROS in May 2010, the first successful solar sail mission, denoted the emergence of the engineering stage of solar sail technology. In fact, many research institutes, such as NASA, JAXA, ESA, and DLR, have started projects to develop solar sail technology. The Japanese IKAROS (Interplanetary Kite-craft Accelerated by Radiation Of the Sun) developed by JAXA is the first successful spacecraft to test the solar radiation pressure as the propellantless propulsion, which was launched into a near-Venus transfer trajectory in May 2010 [1]. In November 2010, the NanoSail-D solar sail craft developed by NASA, which is a small satellite to study the deployment of a solar sail, was successfully launched into a low Earth orbit [2]. In November 2009, DLR and ESA agreed to a 3-step Gossamer road map to solar sailing. The goals of this project are to develop and to demonstrate solar sail technology as a safe, reliable and manageable propulsion technique for long-lasting and deep-space missions [3]. These institutes have implemented a series of solar sail related activities, including a significant amount of theoretical researches and pre-launch experiments [4–7]. The two successful solar sailing demonstrations in space have led to developments of solar sail knowledge and related technologies that can not be acquired by ground-based experiments. Nevertheless, some of the key technologies of solar sails are still immature, including the solar sail craft design and manufacturing process, trajectory optimization, and attitude control. In fact, the launching of demonstration flights brings new challenges to theoretical studies, which are now being requested to be more practical and detailed.

In deep space exploration, the attractive advantage of using solar sails is its propellantless propulsion. Therefore,

through solar sailing, orbital maneuvers and interplanetary transfers can be performed without consuming any fuel. In general, because the solar radiation pressure force is rather small, the deep space flight time is relatively long. As a result, trajectory optimization to achieve the minimum flight time based on solar sailing is hurry.A number of studies on solar-sailing-based interplanetary missions were performed in the late 1970s, with on the most notable being the study of a rendezvous with Comet Halley in 1986 [8]. Sauer [9] presented detailed trajectory designs, based upon a generalized variational approach, assuming the orbits of Earth and Mars to be circular and coplanar. Lebedev and Zhukov [10] first investigated the time-optimal transfer from Earth to Mars using a solar sail. Jayaraman [11] revisited the minimum-time transfers between the orbits of Earth and Mars using different characteristic accelerations. Jayaraman's solutions were different from those obtained by Lebedev and Zhukov. Jayaraman's transfer times were approximately 10% larger and his sail orientation histories were significantly different to the results of Lebedev and Zhukov. Wood et al. [12] commented on the work of Jayaraman, indicating that the solutions in Ref. [11] were correct and the transversality condition of variational calculus had been applied incorrectly. Indirect methods are quite conventional and available for solving trajectory optimization problems, and in many literatures some practical details of indirect methods were discussed [13–16]. In recent years, many trajectory optimization studies of solar sailing exploration missions have been reported. Hughes and Macdonald [17] studied a Mercury sample return mission using solar sail propulsion and provided details of the mission and a trajectory analysis. Mengali and Quarta [18] investigated the potential offered by a solar-sail-based rendezvous mission toward Asteroid 99942 Apophis, using an optical solar sail model to determine the rapid transfer trajectories. In this paper, for an ideal flat solar sail, the transfer time for rendezvous mission is optimized over a restricted cone-angle range, and an optimal control model will be proposed by using an indirect method for the optimization problem.

2 Optimal control model to determine the minimum rendezvous transfer time

Consider the problem of minimizing the transfer time of interplanetary rendezvous mission. In this paper, an ideal, perfectly reflecting flat sail is assumed. The lightness number β is used to describe the solar sail performance of the solar radiation pressure acceleration. A cone angle α and a clock angle δ are used to define the orientation of the solar sail. As shown in Fig. 1, the cone angle α is defined as the angle between the sail surface normal $\boldsymbol{n}$ and the incident radiation direction, and the clock angle δ is defined as the angle between the solar sail heliocentric angular momentum $\boldsymbol{h}$ and the projection of $\boldsymbol{n}$ onto the plane normal to the radial direction of solar sail. Therefore, the unit vector of the sail surface normal $\boldsymbol{n}$ may be written as

$$\hat{\boldsymbol{n}} = \cos\alpha\hat{\boldsymbol{r}} + \sin\alpha\cos\delta\hat{\boldsymbol{h}} + \sin\alpha\sin\delta\hat{\boldsymbol{t}}, \tag{1}$$

where the unit vectors $\hat{\boldsymbol{r}}$, $\hat{\boldsymbol{h}}$, and $\hat{\boldsymbol{t}}$ are along the radial, orbit normal and transverse directions, respectively. The vectors with a symbol "^" denotes the unit vectors. Therefore, the solar radiation pressure force can be written as

$$\boldsymbol{F}_{\mathrm{SRP}} = \beta\frac{\mu_{\mathrm{S}}}{r^2}\cos^2\alpha\hat{\boldsymbol{n}}, \tag{2}$$

where μ_{S} is the solar gravitational constant, and r is the heliocentric distance of solar sail, and β is the lightness number of the solar sail..

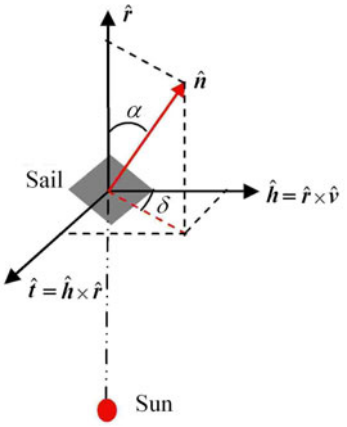

Fig. 1 Definitions of the cone angle and the clock angle for solar sails

2.1 Equations of motion

Considering the two-body model with no perturbations, the forces exerted on the solar sail are solar gravity and the force due to solar radiation pressure. Then, the solar sail dynamic equation is given by

$$\begin{aligned}\dot{\boldsymbol{r}} &= \boldsymbol{v},\\ \dot{\boldsymbol{v}} &= -\frac{\mu_{\mathrm{S}}}{r^3}\boldsymbol{r} + \boldsymbol{F}_{\mathrm{SRP}}.\end{aligned} \tag{3}$$

For convenience in calculations, the solar gravitational constant μ_{S} is normalized to 1 when the distance unit is the non-dimensional astronomical unit (AU). Correspondingly, the non-dimensional time unit is used, 1 year being equivalent to 2π nondimensional units. Therefore, the nondimensional equations of motion for an ideal solar sail in the heliocentric ecliptic inertial frame can be given as

$$\begin{aligned}\dot{\boldsymbol{R}} &= \boldsymbol{V},\\ \dot{\boldsymbol{V}} &= -\frac{1}{R^3}\boldsymbol{R} + \beta\frac{1}{R^2}\cos^2\alpha\hat{\boldsymbol{n}},\end{aligned} \tag{4}$$

where $\boldsymbol{R}$ and $\boldsymbol{V}$ are the nondimensional position and velocity vectors. For an ideal solar sail, the control variable is the unit sail normal vector $\hat{\boldsymbol{n}}$, which is equivalent to the sail attitude angles α and δ according to the definition of Eq. (1).

In general, the cone angle can change from 0° to 90°. In this study, we consider the case in which the cone angle

range is restricted less than an acute angle. The maximum cone angle is indicated as $\alpha_{\max}$. Therefore, the control variables satisfy the following constraints

$$\hat{\boldsymbol{n}}(t) \in \{\alpha(t), \delta(t) | 0^\circ \leqslant \alpha(t) \leqslant \alpha_{\max} < 90^\circ, \quad 0^\circ \leqslant \delta(t) \leqslant 360^\circ\}. \tag{5}$$

In this case, the sail normal vector $\hat{\boldsymbol{n}}$ can change in a cone, but not in a full half plane.

2.2 Initial and terminal constraints

Consider the interplanetary rendezvous problem of solar sailing, with the solar sail's departure time from the start launch planet/asteroid being t_0 and the rendezvous time to the target planet/asteroid being t_{f}. Assume that the solar sail departs from the heliocentric orbit of the launch planet/asteroid, so the position $\boldsymbol{R}(t_0)$ and velocity $\boldsymbol{V}(t_0)$ of the sail at t_0 are the same as those of the start launch planet/asteroid $\boldsymbol{R}_{\mathrm{start}}(t_0)$ and $\boldsymbol{V}_{\mathrm{start}}(t_0)$; then the initial state constraint can be described as

$$\boldsymbol{\Psi}(t_0) = \begin{bmatrix} \boldsymbol{R}(t_0) - \boldsymbol{R}_{\mathrm{start}}(t_0) \\ \boldsymbol{V}(t_0) - \boldsymbol{V}_{\mathrm{start}}(t_0) \end{bmatrix} = \boldsymbol{0}. \tag{6}$$

At the final time t_{f} for a rendezvous mission, the sail craft's final position $\boldsymbol{R}(t_{\mathrm{f}})$ and velocity $\boldsymbol{V}(t_{\mathrm{f}})$ should be the same as those of the target planet/asteroid $\boldsymbol{R}_{\mathrm{end}}(t_{\mathrm{f}})$ and $\boldsymbol{V}_{\mathrm{end}}(t_{\mathrm{f}})$, so the terminal state constraint is

$$\boldsymbol{\Psi}(t_{\mathrm{f}}) = \begin{bmatrix} \boldsymbol{R}(t_{\mathrm{f}}) - \boldsymbol{R}_{\mathrm{end}}(t_{\mathrm{f}}) \\ \boldsymbol{V}(t_{\mathrm{f}}) - \boldsymbol{V}_{\mathrm{end}}(t_{\mathrm{f}}) \end{bmatrix} = \boldsymbol{0}. \tag{7}$$

Thus, Eqs. (6) and (7) define the state boundary condition.

The initial and final time constraints are given by a 4-D inequality function.

$$\boldsymbol{\sigma} = \begin{bmatrix} t_{0\min} - t_0 \\ t_0 - t_{0\max} \\ t_{\mathrm{f}\min} - t_{\mathrm{f}} \\ t_{\mathrm{f}} - t_{\mathrm{f}\max} \end{bmatrix} \leqslant \boldsymbol{0}, \tag{8}$$

where $t_{0\min}$ and $t_{0\max}$ are the minimum and maximum initial times, and t_{fmin} and t_{fmax} are the minimum and maximum final times.

2.3 Optimal control law

For a solar sail, no fuel is consumed. As a result, the flight time is usually used as the optimization index. Thus the optimal control problem is to minimize the flight time, and the objective function is given by

$$\arg\left(\min\left(J = \int_{t_0}^{t_{\mathrm{f}}} \lambda_0 \mathrm{d}t\right)\right), \tag{9}$$

where t_0 and t_{f} denote the initial and the final times, respectively. The positive weight factor λ_0 is used for normalization, which will be discussed later.

According to the proposed indirect method, the optimal control problem can be transformed into a two-point boundary-value problem by using Pontryagin's minimum principle. By introducing the costate vector $\boldsymbol{\lambda} \triangleq (\boldsymbol{\lambda}_R; \boldsymbol{\lambda}_V)$, the Hamiltonian function of the system is defined as

$$H = \lambda_0 + \boldsymbol{\lambda}_R \cdot \boldsymbol{V} + \boldsymbol{\lambda}_V \cdot \left(-\frac{1}{R^3}\boldsymbol{R} + \beta \frac{1}{R^2}\hat{\boldsymbol{n}} \cos^2 \alpha \right). \tag{10}$$

Therefore, the costate differential equations can be given by

$$\begin{aligned} \dot{\boldsymbol{\lambda}}_R &= -\frac{\partial H}{\partial R} = \frac{1}{R^3}\lambda_V - \frac{3}{R^5}(\boldsymbol{R} \cdot \boldsymbol{\lambda}_V)R \\ &\quad -2\beta \frac{\cos\alpha}{R^3}(\boldsymbol{\lambda}_V \cdot \hat{\boldsymbol{n}})\left(\hat{\boldsymbol{n}} - 2\frac{\boldsymbol{R}}{R}\cos\alpha\right), \\ \dot{\lambda}_V &= -\frac{\partial H}{\partial V} = -\lambda_R. \end{aligned} \tag{11}$$

According to optimal control theory, the initial and terminal costates should satisfy the transversality condition

$$\begin{aligned} \boldsymbol{\lambda}_R(t_0) &= -\frac{\partial^{\mathrm{T}}\boldsymbol{\Psi}(t_0)}{\partial \boldsymbol{R}(t_0)}\boldsymbol{\gamma}_{R_0} = -\boldsymbol{\gamma}_{R_0}, \\ \boldsymbol{\lambda}_V(t_0) &= -\frac{\partial^{\mathrm{T}}\boldsymbol{\Psi}(t_0)}{\partial \boldsymbol{V}(t_0)}\boldsymbol{\gamma}_{V_0} = -\boldsymbol{\gamma}_{V_0}, \end{aligned} \tag{12}$$

$$\begin{aligned} \boldsymbol{\lambda}_R(t_{\mathrm{f}}) &= -\frac{\partial^{\mathrm{T}}\boldsymbol{\Psi}(t_{\mathrm{f}})}{\partial \boldsymbol{R}(t_{\mathrm{f}})}\boldsymbol{\gamma}_{R_{\mathrm{f}}} = -\boldsymbol{\gamma}_{R_{\mathrm{f}}}, \\ \boldsymbol{\lambda}_V(t_{\mathrm{f}}) &= -\frac{\partial^{\mathrm{T}}\boldsymbol{\Psi}(t_{\mathrm{f}})}{\partial \boldsymbol{V}(t_{\mathrm{f}})}\boldsymbol{\gamma}_{V_{\mathrm{f}}} = -\boldsymbol{\gamma}_{V_{\mathrm{f}}}, \end{aligned} \tag{13}$$

where $\boldsymbol{\gamma}_0 = (\boldsymbol{\gamma}_{R_0}; \boldsymbol{\gamma}_{V_0})$ and $\boldsymbol{\gamma}_{\mathrm{f}} = (\boldsymbol{\gamma}_{R_{\mathrm{f}}}; \boldsymbol{\gamma}_{V_{\mathrm{f}}})$ are undetermined Lagrange multiplier vectors.

In addition, the Hamiltonian function at both the initial and final times should satisfy the stationarity condition

$$\begin{aligned} H(t_0) &= \boldsymbol{\gamma}_0 \cdot \frac{\partial \boldsymbol{\Psi}(t_0)}{\partial t_0} \\ &= -\boldsymbol{\gamma}_{R_0} \cdot \boldsymbol{V}_{\mathrm{start}}(t_0) - \boldsymbol{\gamma}_{V_0} \cdot \left(-\frac{\boldsymbol{R}_{\mathrm{start}}(t_0)}{R^3_{\mathrm{start}}(t_0)} \right) \\ &= \boldsymbol{\lambda}_R(t_0) \cdot \boldsymbol{V}_{\mathrm{start}}(t_0) - \boldsymbol{\lambda}_V(t_0) \cdot \frac{\boldsymbol{R}_{\mathrm{start}}(t_0)}{R^3_{\mathrm{start}}(t_0)}, \end{aligned} \tag{14}$$

$$\begin{aligned} H(t_{\mathrm{f}}) &= \boldsymbol{\gamma}_{\mathrm{f}} \cdot \frac{\partial \boldsymbol{\Psi}(t_{\mathrm{f}})}{\partial t_{\mathrm{f}}} \\ &= -\boldsymbol{\gamma}_{R_{\mathrm{f}}} \cdot \boldsymbol{V}_{\mathrm{end}}(t_{\mathrm{f}}) - \boldsymbol{\gamma}_{V_{\mathrm{f}}} \cdot \left(-\frac{\boldsymbol{R}_{\mathrm{end}}(t_{\mathrm{f}})}{R^3_{\mathrm{end}}(t_{\mathrm{f}})} \right) \\ &= \boldsymbol{\lambda}_R(t_{\mathrm{f}}) \cdot \boldsymbol{V}_{\mathrm{end}}(t_{\mathrm{f}}) - \boldsymbol{\lambda}_V(t_{\mathrm{f}}) \cdot \frac{\boldsymbol{R}_{\mathrm{end}}(t_{\mathrm{f}})}{R^3_{\mathrm{end}}(t_{\mathrm{f}})}. \end{aligned} \tag{15}$$

Note that in Eqs. (14) and (15), the undetermined Lagrange multiplier vectors $\boldsymbol{\gamma}_0$ and $\boldsymbol{\gamma}_{\mathrm{f}}$ are replaced by the initial and the final costate vectors $\boldsymbol{\lambda}(t_0)$ and $\boldsymbol{\lambda}(t_{\mathrm{f}})$, respectively, according to Eqs. (12) and (13).

The extremum condition of the two-point boundary-value problem according to Pontryagin's minimum principle is then given by

$$\arg(\min_{\hat{\boldsymbol{n}}}(H)) = \lambda_0 + \boldsymbol{\lambda}_R \cdot \boldsymbol{V} + \boldsymbol{\lambda}_V \cdot \left(-\frac{1}{R^3}\boldsymbol{R} + \beta \frac{1}{R^2}\hat{\boldsymbol{n}} \cos^2 \alpha \right). \quad (16)$$

If the cone angle α is not restricted, i.e., it can be changed from 0° to 90°, the optimal control law can be obtained by the variational method, and the optimal control law can be written as

$$\alpha^* = \begin{cases} 90^\circ, & \tilde{\alpha} = 0^\circ, \\ \tan^{-1}\left(\dfrac{3 + \sqrt{9 + 8\tan^2\tilde{\alpha}}}{4\tan\tilde{\alpha}}\right), & 0^\circ < \tilde{\alpha} < 90^\circ, \\ \tan^{-1}\left(\dfrac{\sqrt{2}}{2}\right), & \tilde{\alpha} = 90^\circ, \\ \tan^{-1}\left(\dfrac{3 - \sqrt{9 + 8\tan^2\tilde{\alpha}}}{4\tan\tilde{\alpha}}\right), & 90^\circ < \tilde{\alpha} < 180^\circ, \\ 0^\circ, & \tilde{\alpha} = 180^\circ, \end{cases} \quad (17)$$

$$\delta^* = 180^\circ + \tilde{\delta},$$

where α^* and δ^* are the optimal control angles of solar sails, and $\tilde{\alpha}$ and $\tilde{\delta}$ are the angles that describe the orientation of unit vector along the velocity costate vector. The definition of the angles are given by

$$\hat{\boldsymbol{\lambda}}_V = \hat{\boldsymbol{r}}\cos\tilde{\alpha} + \hat{\boldsymbol{h}}\sin\tilde{\alpha}\cos\tilde{\delta} + \hat{\boldsymbol{t}}\sin\tilde{\alpha}\sin\tilde{\delta}$$

$$(0^\circ \leqslant \tilde{\alpha} \leqslant 180^\circ, 0^\circ \leqslant \tilde{\delta} < 360^\circ), \quad (18)$$

where the unit vectors $\hat{\boldsymbol{r}}$, $\hat{\boldsymbol{h}}$, and $\hat{\boldsymbol{t}}$ are the same as those used in Eq. (1) and shown in Fig. 1. Generally, the velocity costate vector $\boldsymbol{\lambda}_V$ is called the "Primer Vector" in low-trust trajectory optimization [13]. For an unrestricted cone angle problem, the optimal cone angle changes with the cone angle of the primer vector, and the relationship between them is illustrated in Fig. 2.

However, in this study, the cone angle is assumed to be restricted over a particular acute range. Then, the optimal control law can not be obtained by the variational method, and Pontryagin's minimum principle must be used. Therefore, to minimize the Hamiltonian function for a cone-angle range restricted problem, the optimal control law has different forms for different maximum restricted cone angle ranges. For an unrestricted cone angle problem, the optimal control cone angle has a demarcation point of $\alpha_{\text{crit}} = \arctan\dfrac{\sqrt{2}}{2}(\tilde{\alpha} = 90^\circ)$. Thus, for the cone angle range restricted problem, the maximum restricted cone angle should also take this angle as the cut-off point. Then, for different maximum restricted cone angles, the optimal control law for the restricted cone-angle problem can be given by Eqs. (19) and (20).

if $\alpha_{\max} > \tan^{-1}\dfrac{\sqrt{2}}{2} = 35.26^\circ$,

$$\alpha^* = \begin{cases} \alpha_{\max}, & 0^\circ \leqslant \tilde{\alpha} \leqslant \tan^{-1}\left(\dfrac{3\tan\alpha_{\max}}{2\tan^2\alpha_{\max} - 1}\right), \\ \tan^{-1}\left(\dfrac{3 + \sqrt{9 + 8\tan^2\tilde{\alpha}}}{4\tan\tilde{\alpha}}\right), & \tan^{-1}\dfrac{3\tan\alpha_{\max}}{2\tan^2\alpha_{\max} - 1} < \tilde{\alpha} < 90^\circ, \\ \tan^{-1}\left(\dfrac{\sqrt{2}}{2}\right), & \tilde{\alpha} = 90^\circ, \\ \tan^{-1}\left(\dfrac{3 - \sqrt{9 + 8\tan^2\tilde{\alpha}}}{4\tan\tilde{\alpha}}\right), & 90^\circ < \tilde{\alpha} < 180^\circ, \\ 0^\circ, & \tilde{\alpha} = 180^\circ, \end{cases} \quad (19)$$

$$\delta^* = \tilde{\delta} + 180^\circ,$$

if $\alpha_{\max} < \tan^{-1}\dfrac{\sqrt{2}}{2} = 35.26^\circ$,

$$\alpha^* = \begin{cases} \alpha_{\max}, & 0^\circ \leqslant \tilde{\alpha} \leqslant \tan^{-1}\dfrac{3\tan\alpha_{\max}}{2\tan^2\alpha_{\max} - 1} + 180^\circ, \\ \tan^{-1}\left(\dfrac{3 - \sqrt{9 + 8\tan^2\tilde{\alpha}}}{4\tan\tilde{\alpha}}\right), & \tan^{-1}\dfrac{3\tan\alpha_{\max}}{2\tan^2\alpha_{\max} - 1} + 180^\circ < \tilde{\alpha} < 180^\circ, \\ 0^\circ, & \tilde{\alpha} = 180^\circ, \end{cases} \quad (20)$$

$$\delta^* = \tilde{\delta} + 180^\circ.$$

The optimal cone angle α versus the cone angle of primer vector $\tilde{\delta}$ is shown in Fig. 2 for different maximum restricted cone angles.

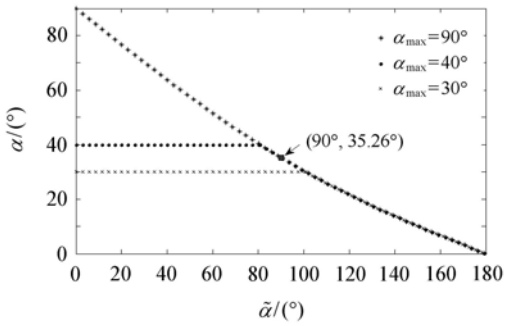

Fig. 2 Optimal sail cone angles α as a function of $\tilde{\alpha}$ for different $\alpha_{\max}$ values

In addition, according to the definition of the sail normal vector $\hat{\boldsymbol{n}}$ and the primer vector $\hat{\boldsymbol{\lambda}}_V$, namely Eqs. (1) and (18), and the optimal control angles, namely Eqs. (19) and (20), the optimal control normal vector can easily be obtained as a function of sail position vector and primer vector as

$$\begin{aligned}\hat{\boldsymbol{n}}^* &= \hat{\boldsymbol{r}}\cos\alpha - \sin\alpha\left(\frac{1}{\sin\tilde{\alpha}}\hat{\boldsymbol{\lambda}}_V - \frac{\cos\tilde{\alpha}}{\sin\tilde{\alpha}}\hat{\boldsymbol{r}}\right)\\ &= \frac{\sin(\tilde{\alpha}+\alpha)}{\sin\tilde{\alpha}}\hat{\boldsymbol{r}} - \frac{\sin\alpha}{\sin\tilde{\alpha}}\hat{\boldsymbol{\lambda}}_V. \end{aligned} \tag{21}$$

It can be seen that the optimal control normal vector $\hat{\boldsymbol{n}}^*$ should be in the same plane spanned by the sail position vector $\hat{\boldsymbol{r}}$ and the primer vector $\hat{\boldsymbol{\lambda}}_V$, as shown in Fig. 3.

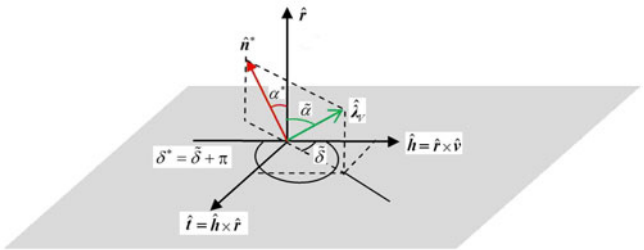

Fig. 3 Optimal control normal vector $\hat{\boldsymbol{n}}^*$

It should be noted that the optimal control law discussed above is applicable to the ideal solar sail model. Although the cone angle range is restricted, essentially the value of cone angle is always changing continuously without jumping (Fig. 2). For the nonideal solar sail model, the optimal cone angle may also change in a particular range. However, it is notable that these two cone angle range restricted cases are quite different: the former is artificially limited, while the latter restriction is determined by the optimal control law. Especially, the cone angle for nonideal sails may change discontinuously when the cone angle of primer vector $\tilde{\alpha}$ is large, and in that case the optimal cone angle may jump to 90° sometimes (it is equivalent to closing the sail film with zero thrust) [19, 20]. However, for the ideal restricted model in this paper, the zero thrust is excluded in the optimal control law, so the optimal cone angle will never be 90° (or jump to 90° from a particular acute angle). Generally, the nonideal sail is different from the ideal sail in dynamics, especially for the zero thrust case. It would be valuable and interesting to solve the optimal problem with the cone angle range restricted artificially for nonideal solar sails, which will be discussed in future.

2.4 Normalization of the initial costate vector

According to the discussion in the previous sections, the time-optimal rendezvous problem is transformed into a two-point boundary-value problem by using an indirect method. For the 12 dimensions of differential equations, including the state and costate equations, namely Eqs. (4) and (11), respectively, the key is to find the initial values for the differential equations to meet the constraints on both the initial and terminal times, namely Eqs. (6), (7), (14) and (15). However, for the shooting functions, the solution is quite sensitive to the change of the initial values; thus, estimating the initial values is difficult. The method of normalization of the initial costates proposed by Jiang et al. [16] is quite useful for the estimation of the initial costates. According to Jiang's method, all the initial costate values can be turned into bounded ranges, and this normalization method has no effect on the results but simplifies the estimation of the initial values. Here, to include the positive weight factor λ_0 introduced in the objective function of Eq. (9), the normalized multiplier vector is written as

$$\boldsymbol{\lambda} = \frac{\boldsymbol{\lambda}}{\|\boldsymbol{\lambda}(t_0)\|} = \frac{(\lambda_0;\boldsymbol{\lambda}_R;\boldsymbol{\lambda}_V)}{\|(\lambda_0;\boldsymbol{\lambda}_R(t_0);\boldsymbol{\lambda}_V(t_0))\|}, \tag{22}$$

where the positive weight factor λ_0 does not vary with time. So the normalization of the initial costate vector should satisfy the following requirement

$$\|\boldsymbol{\lambda}(t_0)\| = \sqrt{\lambda_0^2 + \boldsymbol{\lambda}_R(t_0)\cdot\boldsymbol{\lambda}_R(t_0) + \boldsymbol{\lambda}_V(t_0)\cdot\boldsymbol{\lambda}_V(t_0)} = 1. \tag{23}$$

Introducing six angles, the 7-D initial costate values can be transformed as

$$\begin{aligned}&\lambda_0 = \sin\alpha_1,\\ &\boldsymbol{\lambda}_R(t_0) =\\ &\quad\cos\alpha_1\cos\alpha_2(\cos\alpha_3\cos\alpha_4;\cos\alpha_3\sin\alpha_4;\sin\alpha_3),\\ &\boldsymbol{\lambda}_V(t_0) =\\ &\quad\cos\alpha_1\sin\alpha_2(\cos\alpha_5\cos\alpha_6;\cos\alpha_5\sin\alpha_6;\sin\alpha_5).\end{aligned} \tag{24}$$

According to Eq. (24), the normalization condition of the initial costate is met naturally. To satisfy the positivity of the weight factor λ_0 and the unrestricted nature of other costates, the value range of the six angles should be

$$\begin{aligned}
&\alpha_{1,2} = \frac{\pi}{2}X_{1,2} \in \left[0, \frac{\pi}{2}\right],\\
&\alpha_{3,5} = \pi\left(X_{3,5} - \frac{1}{2}\right) \in \left[-\frac{\pi}{2}, \frac{\pi}{2}\right],\\
&\alpha_{4,6} = 2\pi X_{4,6} \in [0, 2\pi].
\end{aligned} \tag{25}$$

Similarly, the initial time t_0 and terminal time t_f can be obtained by two values $X_{7,8}$ with a range of [0, 1] according to the time constraints of Eq. (8)

$$\begin{aligned}
&t_0 = t_{0\,\min} + X_7(t_{0\,\max} - t_{0\,\min}) \in [t_{0\,\min}, t_{0\,\max}],\\
&t_f = t_{f\min} + X_8(t_{f\max} - t_{f\min}) \in [t_{f\min}, t_{f\max}].
\end{aligned} \tag{26}$$

Therefore, to solve the two-point boundary-value problem, including the initial and terminal time and the indeterminate initial costates (λ_0; $\boldsymbol{\lambda}_R(t_0)$; $\boldsymbol{\lambda}_V(t_0)$), the total of nine unknowns required to be estimated to meet the shooting functions are transformed to eight values X_{1-8}, each over the range of [0, 1]. The boundedness of the variables is quite convenient for numerical calculation. This convenience is particularly true for the present problem, which is sensitive to the initial values, so this method of normalization is conducive to obtain convergent solutions faster.

3 Examples

In this section, numerical solutions of example missions of the minimum transfer time rendezvous problem are described. The sail loading parameter is $\beta = 0.08$, and the solar sail model is ideal, which involves only the solar gravity force and radiation pressure force. All the planets/asteroids are described by two-body motion, and the reference orbital elements, which are all taken at the time of 1st Jan. 2000 (MJD51544.0), are listed in Table 1.

The initial time range is between 1st Jan. 2015 (MJD57 023.0) and 1st Jan. 2016 (MJD57 388.0), and the flight time range is between 600 days and 900 days. Therefore, the initial time and terminal time constraints of Eq. (8) are given as

$$\begin{aligned}
&t_{0\,\min} = 57\,023.0\ \text{(MJD)}, \quad t_{0\,\max} = 57\,388.0\ \text{(MJD)},\\
&t_{f\min} = 57\,623.0\ \text{(MJD)}, \quad t_{f\max} = 58\,288.0\ \text{(MJD)}.
\end{aligned} \tag{27}$$

The example missions all involve departure from Earth, and rendezvous with Mars or Asteroid No. 68278, whose orbital parameters are listed in Table 1. Examples with different restricted maximum cone angle conditions are calculated, and the results are compared and discussed.

3.1 Example of a rendezvous with Mars

The solar sail departs from Earth and has a rendezvous with Mars. The maximum restricted cone angles considered are 30°, 40°, 50°, and 90° (equivalent to being unrestricted), and the key data of the results are listed in Table 2.

The time-varying optimal control angles for different conditions are shown in Fig. 4, and all the transfer trajectories of solar sail are also shown in Fig. 5.

3.2 Example of a rendezvous with Asteroid No. 68278

The solar sail departs from Earth and has a rendezvous with Asteroid No. 68278. The maximum restricted cone angles considered are 45°, 50°, 55°, and 90° (equivalent to being unrestricted), and the key data of the results are listed in Table 3.

The time-varying optimal control angles for different conditions are shown in Fig. 6, and all the transfer trajectories of the solar sail are shown in Fig. 7.

4 Discussions and conclusions

According to the optimal results of the examples in Sect. 3, the values of the maximum restricted cone angle have effects on the optimal flight time and the transfer trajectories. The results indicate that for the condition of a restricted cone-angle range, the transfer time of an optimal rendezvous is longer than that of the unrestricted case, and with the decrease of the maximum restricted cone angle, the optimal rendezvous transfer time will increase correspondingly. Since the optimal control angles vary with time, excessive cone angles are seemingly set to the maximum values for the

Table 1 The reference orbital elements of the target planets/asteroids

	a/AU	e	i/(°)	Ω/(°)	ω/(°)	f/(°)
Earth	1.000 588 177 3	0.016 195 088 5	0.002 123 743 2	139.022 629 133 4	−34.572 476 170 0	2.655 488 898 1
Mars	1.523 677 158 9	0.093 435 242 5	1.849 298 927 3	49.538 447 543 8	−73.438 413 476 7	19.069 275 430 6
Asteroid No. 68278	1.435 718 701 8	0.114 487 026 2	2.620 615 528 6	99.140 785 434 1	−125.665 842 013 7	−39.971 606 409 0

Table 2 The optimal results of a rendezvous with Mars

$\alpha_{\max}$/(°)	λ_0	$\boldsymbol{\lambda}_R(t_0)$	$\boldsymbol{\lambda}_V(t_0)$	Depart date	Rendezvous date	Flight time/d
30	0.014 1	(−0.555 6; −0.468 6; 0.075 2)	(−0.425 4; −0.510 9; −0.154 6)	09/24/2015	10/19/2017	755.81
40	0.013 4	(−0.408 4; −0.639 6; 0.003 6)	(−0.227 5; −0.571 4; −0.213 8)	10/13/2015	08/24/2017	681.36
50	0.012 8	(−0.322 8; −0.699 2; −0.046 7)	(−0.124 2; −0.568 1; −0.257 6)	10/21/2015	08/16/2017	665.26
90	0.012 2	(0.320 7; 0.689 3; 0.052 3)	(0.045 7; 0.577 2; 0.289 6)	10/23/2015	08/14/2017	660.80

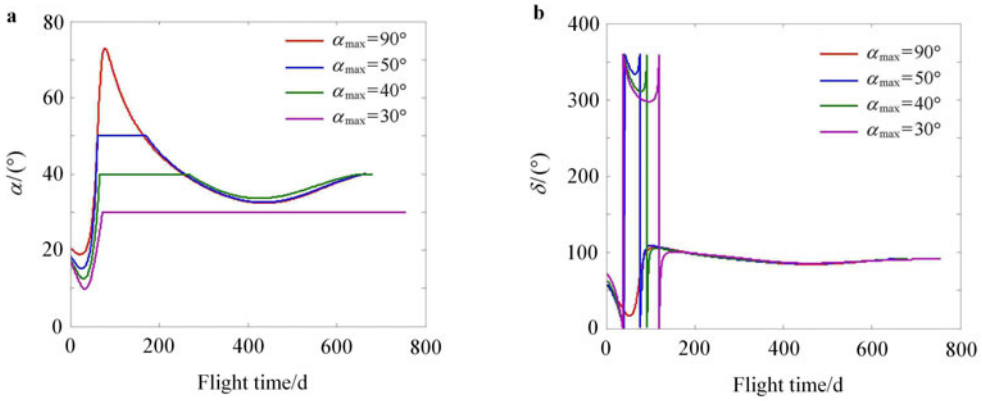

Fig. 4 The optimal control angles of a rendezvous with Mars

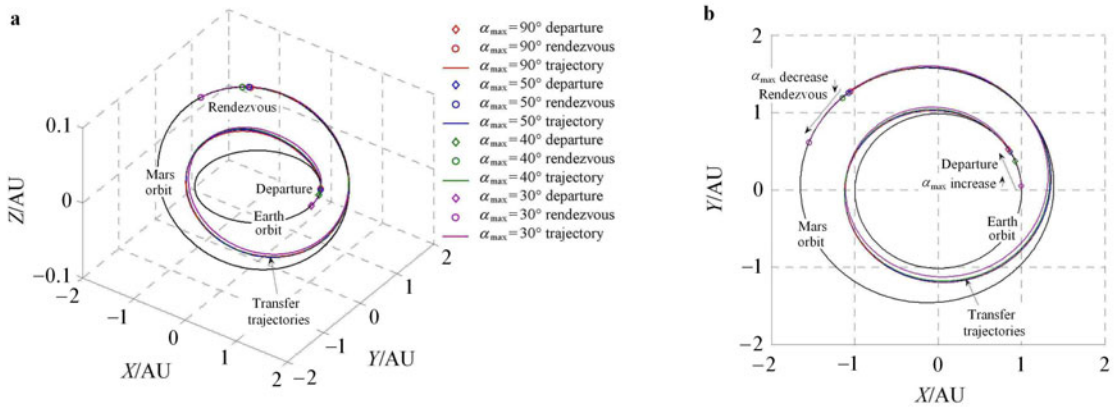

Fig. 5 The optimal transfer trajectories of a rendezvous with Mars. **a** 3-D View; **b** *XY* Plane

Table 3 The optimal results of a rendezvous with Asteroid No. 68278

$\alpha_{max}/(°)$	λ_0	$\boldsymbol{\lambda}_R(t_0)$	$\boldsymbol{\lambda}_V(t_0)$	Depart date	Rendezvous date	Flight time/d
45	0.002 8	(0.688 8; 0.3304; −0.140 2)	(−0.592 5; 0.172 8; 0.113 4)	05/07/2015	03/10/2017	672.84
50	0.002 7	(0.711 2; 0.290 3; −0.167 2)	(−0.574 2; 0.191 5; 0.124 8)	05/04/2015	03/01/2017	667.47
55	0.002 7	(0.717 1; 0.277 1; −0.176 3)	(−0.565 5; 0.199 6; 0.135 0)	05/02/2015	02/26/2017	665.33
90	0.002 7	(−0.719 7; −0.271 7; 0.181 1)	(0.559 0; −0.205 3; −0.144 3)	05/02/2015	02/24/2017	664.71

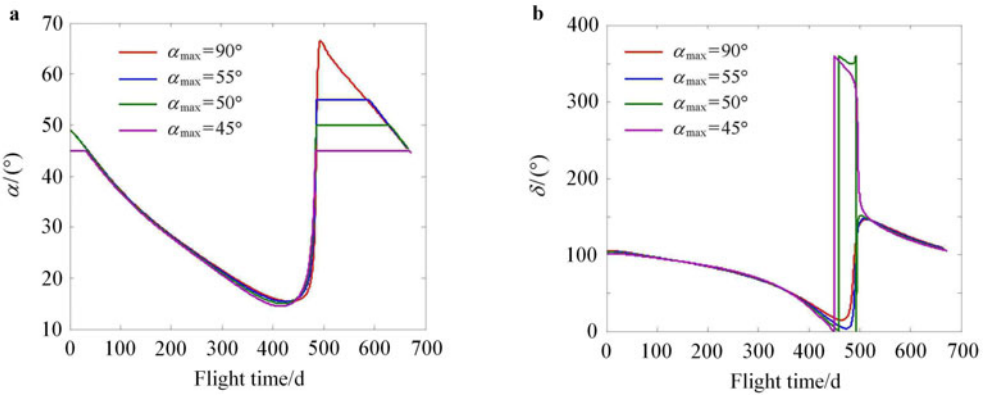

Fig. 6 The optimal control angles of a rendezvous with Asteroid No. 68278

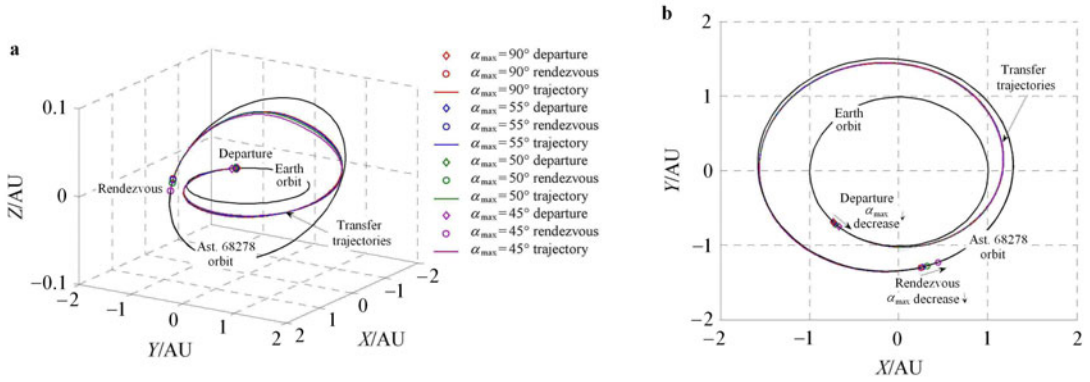

Fig. 7 The optimal transfer trajectories of a rendezvous with Asteroid No. 68278. **a** 3-D View; **b** *XY* Plane

restricted conditions. However, it is not a simple replacement, and for different maximum restricted cone angle conditions, the departure time, rendezvous time, and the total transfer trajectories are different. Note that for different rendezvous target, the relationship between the departure/arrival time and the value of $\alpha_{\max}$ is irregular. It can be seen that, for the mission of a rendezvous with Mars mentioned in Sect. 3.1, with the decrease of the maximum restricted cone angle, the departure time will advance and the rendezvous time will delay correspondingly and vice-versa. However, for the mission of a rendezvous with Asteroid No. 68278, with the decrease of the maximum restricted cone angle, the departure time and the rendezvous time will both delay correspondingly. In addition, due to the sensitivity to the initial values of the indirect method, it is harder to estimate the initial values and to solve the problem for a smaller restricted cone angle. Even worse, if the maximum restricted cone angle is too small (the extreme example is $\alpha_{\max} = 0°$), it may be impossible to achieve a rendezvous with the target planet/asteroid in a limited time; thus, solutions can not be obtained for cone angles that are too small. However, the minimum values of the possible maximum restricted cone angles are different for different missions, and the existence of a solution for the restricted conditions will be discussed in a future study.

References

1 Tsuda, Y., Mori, O., Funase, R., et al.: Flight status of IKAROS deep space solar sail demonstrator. Acta Astronautica **69**, 833–840 (2011)

2 Johnson, L., Whorton, M., Heaton, A., et al.: NanoSail-D: A solar sail demonstration mission. Acta Astronautica **68**, 571–575 (2011)

3 Geppert, U., Biering, B., Lura, F., et al.: The 3-step DLR–ESA Gossamer road to solar sailing. Advances in Space Research **48**, 1695–1701 (2011)

4 Sickinger, C., Herbeck, L., Breitbach, E.: Structural engineering on deployable CFRP booms for a solar propelled sailcraft. Acta Astronautica **58**, 185–196 (2006)

5 Okuizumi, N., Yamamoto, T.: Centrifugal deployment of membrane with spiral folding: Experiment and simulation. Journal of Space Engineering **2**, 41–50 (2009)

6 Quadrelli, M.B., West, J.: Sensitivity studies of the deployment of a square inflatable solar sail with vanes. Acta Astronautica **65**, 1007–1027 (2009)

7 Whorton, M.S.: Solar sail orbit determination from ground observations: A proposed professional-amateur collaboration. Society for Astronomical Sciences Annual Symposium **24**, 97 (2005)

8 Friedman, L., Carroll, W., Goldstein, R., et al.: Solar sailing-The concept made realistic. AIAA Paper 78–82, Jan (1978)

9 Sauer, C.G.: Optimum solar-sail interplanetary trajectories. AIAA Paper 76-792, San Diego, CA, Aug. 18–20 (1976)

10 Zhukov, A.N., Lebedev, V.N.: Variational problem of transfer between heliocentric orbits by means of a solar sail. Kosmicheskie Issledovaniya (Cosmic Research) **2**, 45–50 (1964)

11 Jayaraman, T.S.: Time-optimal orbit transfer trajectory for solar sail spacecraft. Journal of Guidance, Control, and Dynamics **3**, 536–542 (1980)

12 Wood, L.J., Bauer, T.P., Zondervan, K.P.: Comment on "time-optimal orbit transfer trajectory for solar sail spacecraft". Journal of Guidance, Control, and Dynamics **5**, 221–224 (1982)

13 Lawden, D.F.: Optimal Trajectories for Space Navigation. Butterworths, London, 54–68 (1963)

14 Cassenti, B.: Optimisation of interstellar solar sail velocities. Journal of the British Interplanetary Society **50**, 475–478 (1997)

15 Casalino, L., Colasurdo, G., Pastrone, D.: Indirect approach for minimum-fuel aeroassisted transfers. AIAA/AAS Astrodynamics Conference, San Diego, CA (1996)

16 Jiang, F., Baoyin, H., Li, J.: Practical techniques for low-thrust trajectory optimization with homotopic approach. Journal of Guidance, Control, and Dynamics **35**, 245–258 (2012)

17 Hughes, G.W., Macdonald, M., McInnes, C.R., et al.: Sample return from Mercury and other terrestrial planets using solar sail propulsion. Journal of Spacecraft and Rockets **43**, 828–835 (2006)

18 Mengali, G., Quarta, A.A.: Rapid solar sail rendezvous missions to Asteroid 99942 Apophis. Journal of Spacecraft and Rockets **46**, 134–140 (2009)

19 Colasurdo, G., Casalino, L.: Optimal control law for interplanetary trajectories with nonideal solar sail. Journal of Spacecraft and Rockets **40**, 260–265 (2003)

20 Mengali, G., Quarta, A.A.: Optimal three-dimensional interplanetary rendezvous using non-ideal solar sail. Journal of Guidance, Control, and Dynamics **28**, 173–177 (2005)